

A comparison of non-pulsed radiofrequency and pulsed radiofrequency glow discharge orthogonal time-of-flight mass spectrometry for analytical purposes

L. Lobo,^a J. Pisonero,^b N. Bordel,^b R. Pereiro,^a A. Tempez,^c P. Chapon,^c J. Michler,^d M. Hohl^e and A. Sanz-Medel^{*a}

Received 22nd April 2009, Accepted 29th July 2009

First published as an Advance Article on the web 13th August 2009

DOI: 10.1039/b908038d

The analytical potential of a radiofrequency glow discharge orthogonal time-of-flight mass spectrometer (RFGD-TOFMS) has been evaluated in both pulsed and non-pulsed modes. A certified reference steel was selected for this study. The operating conditions of the GD plasma (pressure and applied power) were optimized in terms of sensitivity. Additionally, duty cycle and pulse width parameters were investigated in the pulsed RF mode. In this case, high analyte ion signals and improved signal to background ratios were measured after the end of the pulse, in the so-called afterglow domain. The analyte ion signals were normalized to sputtering rates to compare different operating conditions. It was found that the sensitivity in the pulsed mode was improved in comparison to the non-pulsed mode; however, the factor of enhancement is element dependent. Moreover, improved analytical performance was obtained in terms of ion separation capabilities as well as in terms of accuracy and precision in the evaluation of the isotopic ratios, using the pulsed RFGD-TOFMS. Additionally, depth profile analyses of a Zn/Ni coating on steel were performed and the non-pulsed and pulsed RFGD-TOFMS analytical performances were compared.

Introduction

Glow discharge (GD) spectroscopies allow rapid and sensitive bulk and depth profile analyses.^{1–3} In particular, GDs have gained importance as atomic ionization sources for mass spectrometry (MS) due to the capability of these low pressure plasmas to generate ionic populations directly from solid samples. In this context, radiofrequency (RF) powered GDs have broadened GD-MS applications to the analysis of non-conductive samples due to their ability to sputter both conducting and insulating materials.^{4–6} Fundamentals of the different processes taking place in the RFGD plasmas have already been studied in depth.^{7,8}

So far, GDs have been coupled to different types of mass analysers, such as quadrupole, sector field, or time-of flight (TOF) mass spectrometers, which specifically provide different advantages and drawbacks. Only sector field based GD-MS instruments are commercially available at the moment, providing high sensitive bulk elemental analysis of solid conductive materials (limits of detection in the ng g⁻¹ range). Nevertheless, the use of this instrumentation is not appropriate for thin-film depth profiling of many elements because of its sequential nature of detection. This limitation has been overcome with the development of GD-TOFMS. In particular, RFGD-TOFMS can be

considered a powerful technique for sensitive direct solid analysis and depth profiling with nanometer resolution of a wide variety of materials.^{9,10}

GD-MS is commonly operated in non-pulsed mode, nevertheless pulsed GD-MS has been reported to offer unique analytical characteristics. In particular, different time windows (prepeak, plateau and afterglow) are observed in pulsed GD due to different dominant ionization processes.¹¹ In this way, pulsed GD-TOFMS has been successfully applied for concurrent elemental and molecular analysis of organic compounds in gas phase.^{12,13} In addition, it has been recently shown that some direct solid qualitative information of polymeric films can be obtained using this technique,¹⁴ but in the present paper the authors have focussed on elemental information. In the specific application of pulsed RFGD-MS for direct solid analysis, the prepeak region is observed at the electric breakdown of the plasma gas upon the application of the discharge power. In this time window only ion signal contributions from the discharge gas species are detected. Then, during the plateau, the analyte ions, which are produced upon plasma ionization of sputtered neutrals appear. The afterglow time window is the most interesting from the analytical point of view and arises upon termination of the discharge power. Key phenomena including ionization processes, gas flow dominated ion transport and chemical reactions take place in the spatial and temporal afterglow plasmas.¹⁵

A pulsed or modulated GD coupled to an orthogonal TOFMS offers appropriate selection of gates in the temporal profiles, in such a way that analyte signals are maxima and contaminant and/or isobaric molecular signals (*e.g.* Ar adducts) are minimal.¹⁶ Moreover, pulsed RFGD-TOFMS is particularly advantageous for the analysis of heat sensitive materials, such as glasses⁹ or polymers.¹⁴ Of course, pulsed RFGD allows higher instant

^aDepartment of Physical and Analytical Chemistry, Faculty of Chemistry, University of Oviedo, 33006 Oviedo, Spain

^bDepartment of Physics, Faculty of Science, University of Oviedo, 33007 Oviedo, Spain

^cHoriba Jobin Yvon, Longjumeau, 91160, France

^dEMPA Materials Science and Technology, Feuerwerkerstr. 39, CH-3602 Thun, Switzerland

^eTofwerk AG, Uttigenstrasse 22, CH-3600 Thun, Switzerland

applied powers to improve the ionization/excitation efficiencies, but the average energy per GD period, given by the instantaneous power and the duty cycle, is only a fraction of that used in the non-pulsed RF mode.

The analytical potential of a radiofrequency glow discharge coupled to an orthogonal time of flight mass spectrometer is thoroughly evaluated here, both in non-pulsed and pulsed RF modes. The main operating conditions of the RFGD (*e.g.* pressure and applied power) were optimized using a certified reference steel. Moreover, intrinsic parameters of the pulsed RFGD, such as pulse width and pulse period have been optimized to provide the highest signal to background ratio. Analytical performance characteristics such as reproducibility, accuracy, precision and depth resolving power (in this latter case for the analysis of a thin coated sample) have been investigated and compared using both non-pulsed and pulsed RF modes.

Experimental

The RFGD-TOFMS includes a RFGD bay unit (RF generator, matching box, RF connector, refrigerator disc and sample mounting system with a pneumatic piston to press the sample against the source), from a GD Profiler HR instrument (Horiba Jobin Yvon, Longjumeau, France). The GD source is a copper-based modified Grimm-type chamber with a 4 mm diameter anode and a 2.5 mm inner diameter flow tube (EMPA, Switzerland).¹⁷ The ions originating from the source are then extracted through a sampler of 500 μm diameter and a 1 mm diameter skimmer. The following interface region includes electrostatic focusing and deflecting components and couples the source to a fast orthogonal TOFMS (Tofwerk, Thun, Switzerland) with a microchannel plate detector.

The RF power is supplied to the plasma through the backside of the sample. The radiofrequency power supply (13.56 MHz) can be run either in pulsed mode with a frequency between 0.1 Hz and 10 kHz or in non-pulsed mode. The pulse width can be selected from 50 μs up to several milliseconds and 150 W is the maximum forward power provided by the RF generator. A refrigerating disc in contact with the sample is used to keep the sample at low temperatures ($<5^\circ\text{C}$). Finally, a pneumatic holder is used to press the sample against the GD ion source. Module and phase of the applied RF power were adapted to keep the reflected power to the minimum value in the non-pulsed and pulsed modes.

In the interface between the GD and the TOFMS, two orifices (sampler and skimmer) are used to transport the ions from the high pressure GD plasma into the low pressure mass analyser. In this work the sampler and skimmer orifice diameters are 500 μm and 1000 μm , respectively. The GD source is evacuated using a dry pump (Triscroll 300, Varian Inc., Palo Alto, USA).

The 30 kHz extraction frequency to the flight tube, as employed in this work, provides a complete mass spectrum up to 250 Th in each extraction. To improve the signal-to-noise ratio and the reproducibility of the ion intensities the spectra recorded in non-pulsed RFGD-TOFMS mode are averages of 30 000 TOF extractions collected in 0.99 seconds. Moreover, total acquisition time, which corresponds to the collection of 60 mass spectra, is about 1 minute. These 60 mass spectra are again averaged for data evaluation. In pulsed RFGD-TOFMS, the measured

analyte ion intensities vary along the GD pulse period, defining the pulse profile of all selected mass peaks (at each temporal position of the pulse profile it is possible to extract the corresponding mass spectrum ($<250\text{ Th}$)). In order to improve the signal-to-noise ratio 1400 pulse profiles from 1400 successive GD pulses were averaged (acquisition time of one “average pulse profile” = 1400 GD pulses \times 4 ms GD period = 5.6 s). Therefore, every 5.6 s the mass spectra from all the temporal positions along the GD pulse are collected. The total acquisition time is 67 s from twelve averaged pulse profiles. The last seven ones are averaged for data evaluation in order to assure a stable signal.

The analyte ion signals used to compare the figures of merit of both modes are calculated as the mean value of six different measurements in two different craters of the same sample. The selected pulse frequency was 250 Hz. Pulse widths between 1.5 ms and 2.5 ms were tested.

High purity Ar (99.999% minimum purity) from Air Liquid (Oviedo, Spain) was employed as discharge gas for all the experiments. The NIST 1262b certified reference steel was used to evaluate the analytical performance of the non-pulsed and pulsed RFGD-TOFMS. The detailed composition of this reference material is given in Table 1.

Depth profile analyses of a sample consisting of a Zn/Ni coating on steel were performed by non-pulsed and pulsed RFGD-TOFMS. Crater shapes produced in sample NIST 1262b at the selected conditions were measured in both modes with a profilometer (Perth-o-meter SSP, Mahr Perthen), along two crater diameters each of them in two different directions. Sputtering rates were then evaluated as mass lost per unit time, by using the software “CraterVol”.¹⁸

Results and discussion

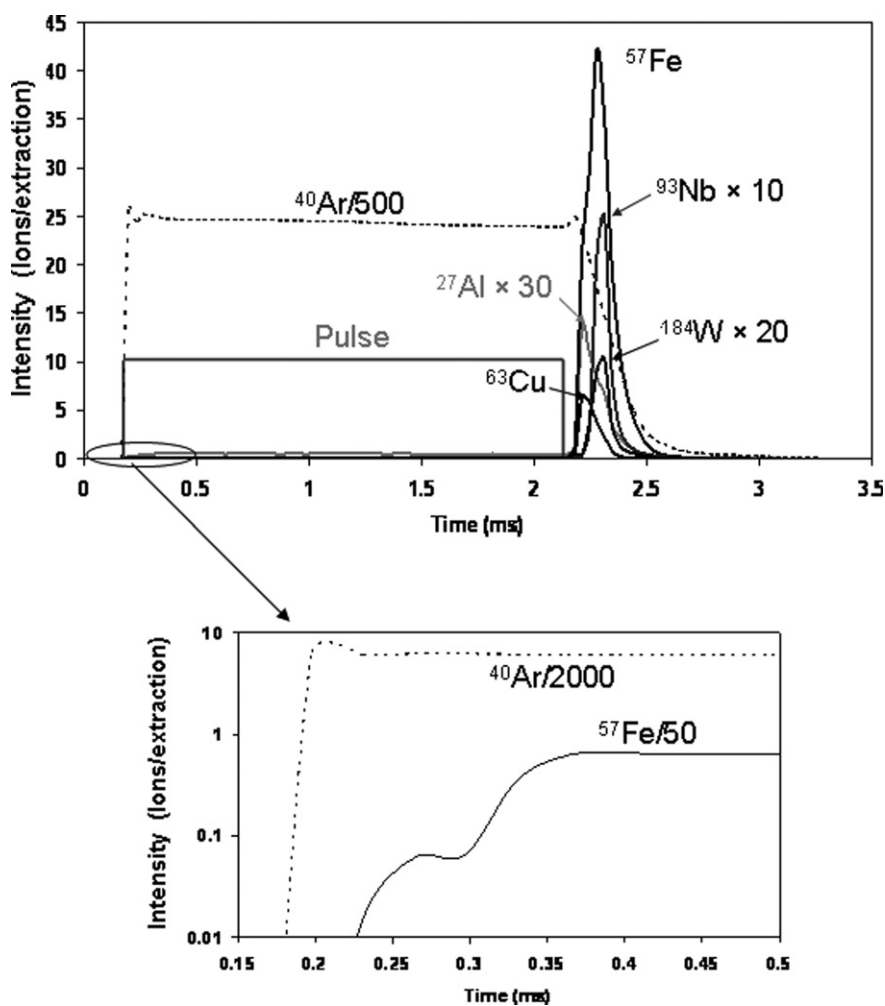
Optimization of the operating conditions

Fig. 1 shows the pulse profiles of $^{40}\text{Ar}^+$ and five analyte ions ($^{27}\text{Al}^+$, $^{57}\text{Fe}^+$, $^{63}\text{Cu}^+$, $^{93}\text{Nb}^+$ and $^{184}\text{W}^+$) of 1262b material obtained using the pulsed RFGD-TOFMS system. The ion response is monitored along 100 successive TOF extractions, with a time resolution of 33 μs (1 TOF extraction = 33 μs). The RF pulse had a duration of 2 ms and 150 μs afterwards delay signal acquisition started. As it has already been described,¹⁵ at the end of the GD pulse Ar^+ recombines with electrons producing a high population of argon metastables (Ar^m). Most of the analyte atoms are ionized through collisions with Ar^m . As a result, an important increase in the analyte ion signals is observed in the afterglow. As can be seen in Fig. 1, not all the analytes have their maxima at the same time: most of the isotopes showed their maxima at 2.28 ms (130 μs after the end of the GD pulse), while the maximum intensity of other isotopes (*e.g.* $^{27}\text{Al}^+$ or $^{63}\text{Cu}^+$) occurred at 61 μs after the end of the GD pulse. The obtained afterglow for the analytes had a temporal duration of 200–300 μs . Moreover, it has been observed the shape of the afterglow varies with the element (as can be seen in Fig. 1) but also with the discharge conditions. For instance, $^{27}\text{Al}^+$ and $^{63}\text{Cu}^+$ besides the early maximum, exhibit a hump in the later afterglow while $^{93}\text{Nb}^+$ and $^{184}\text{W}^+$ present a symmetric afterglow. Previous experiments using pulsed-RF-GD-TOFMS have shown that heavier isotopes tend to exhibit later afterglow peaks and that those delays are not much affected

Table 1 Elemental mass fraction content (%) of the iron reference materials NIST 1262b, 1263a, 1264a and 1265a (Fe content is calculated as the difference to 100%). (*: not certified values)

	Element											
	Ag	Al	As	B	Co	Cr	Cu	Mg	Mn	Mo	Nb	Ni
1262b	0.0011	0.081	0.096	0.0025	0.30	0.30	0.51	0.0006	1.05	0.070	0.30	0.59
1263a	0.0037	0.24	0.010	0.0009	0.048	1.31	0.09	0.00049	1.50	0.030	0.049	0.32
1263a	—	—	0.05	0.011*	0.15	0.06	0.25	0.00015	0.25	0.49	0.15	0.14
1264a	—	0.0007	0.0002*	0.0013	0.007	0.007	0.0058	—	0.0057	0.0050	—	0.041

	Element										
	P	Pb	S	Sb	Si	Sn	Ta	Ti	V	W	Zr
1262b	0.044	0.0004	0.037	0.012	0.40	0.016	0.20	0.100	0.041	0.20	0.22
1263a	0.02	0.0022	0.005	0.002	0.74	0.10	—	0.050	0.31	0.046	0.050
1263a	0.010	0.024	0.025	0.034	0.067	0.008*	0.11	0.24	0.10	0.10	0.069
1264a	0.0011	0.00001	0.0055	—	0.008	—	—	0.0001	0.0006	—	—

**Fig. 1** Pulsed RFGD profiles of $^{27}\text{Al}^+$, $^{57}\text{Fe}^+$, $^{63}\text{Cu}^+$, $^{93}\text{Nb}^+$, $^{184}\text{W}^+$ and ^{40}Ar ions on NIST 1262b standard. Discharge conditions: 100 W, 300 Pa, pulse width: 2 ms and RF period: 4 ms.

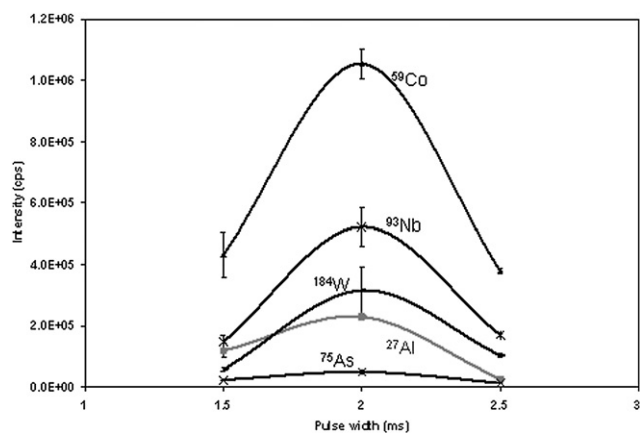


Fig. 2 Ion signal intensities measured for some analytes over the entire afterglow time domain as a function of pulse width at a RF period of 4 ms. Measurements were made at 700 Pa and 80 W on NIST 1262b.

by the applied forward power or pressure.⁹ Further fundamental studies using different matrix samples are needed to fully understand these delays and shape variations.

In the pulsed RF mode, the pulse width was optimised at a constant pulse period of 4 ms, using the standard reference material NIST 1262b. Each pulse duration or pulse width defines a duty cycle (ratio between the pulse width and the pulse period). Three different pulse widths were tested (1.5, 2 and 2.5 ms) over the entire afterglow time domain. As shown in Fig. 2, the best results were obtained at 2 ms pulse width. This value was thus used for the rest of the pulsed RF mode experiments (duty cycle of 50%).

The forward power and pressure were optimised for both operation modes under study. Pressure optimization was carried out at 30 W in non-pulsed RF mode and at 100 W in pulsed RF mode (in this latter case, 100 W refers to the power during the pulse duration, thus, the average power is lower). Fig. 3 shows the relationship between the ion signal intensity (over the entire afterglow time domain) and the pressure in the GD. It can be observed that in non-pulsed RF mode (Fig. 3a) the maximum intensity is obtained between 500 and 600 Pa depending on the analyte. Similarly, Wagatsuma *et al.*¹⁹ using a direct current GD-MS system reported a maximum and then a decrease of the ion signals when the pressure and discharge current were increased (the voltage was kept constant in these studies). The decrease was attributed to collisional losses of ion species when they are transported from the glow region to the mass analyzer. In pulsed RF mode (Fig. 3b) the corresponding ion signal intensities, collected from the afterglow domain, have an element-dependent maximum at about 700–900 Pa (and so, at pressures higher than in the non pulsed mode), except for $^{56}\text{Mn}^+$ and $^{27}\text{Al}^+$ which continuously increased with pressure in the interval assayed.

Fig. 4 shows comparatively relationships between the analyte ion intensity and the forward power in non-pulsed and pulsed RF modes at the optimum pressure conditions. In non-pulsed RF mode (Fig. 4a) it is observed that up to an applied power of 30 W, the ion intensity increases, and then it falls down. On the other hand, in pulsed RF mode (Fig. 4b) higher ion signal

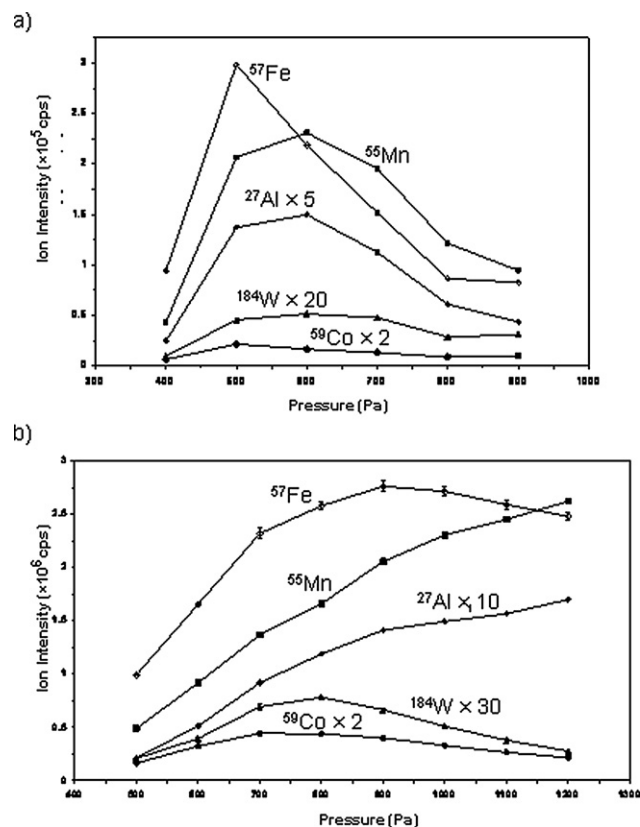


Fig. 3 Ion signal intensities measured for some analytes over the entire afterglow time domain in sample NIST 1262b *versus* pressure. a) non-pulsed RF mode, forward power 30 W; b) pulsed RF mode, forward power 100 W, pulse width: 2 ms, period: 4 ms.

intensities (average values measured in the afterglow) are observed at higher forward power in the interval between 10 and 130 W.

In our RFGD-TOFMS system, it is possible to measure the dc bias developed at the surface of the sample and it has been observed that at increasing applied power values the dc bias is also increased for both non-pulsed and pulsed RF modes. Furthermore, the sputtering rates are also proportional to the applied power in both cases, showing that the atomization process is enhanced at increasing applied powers. Therefore, we believe that lower ion signals observed in non-pulsed-RF mode at higher applied power values could be related to mass load plasma effects (*e.g.* lower ion extraction efficiency through the sampler cone and/or ion losses within the plasma). These mass load plasma effects are significantly different in non-pulsed and pulsed-RF modes, because the plasma is on just a fraction of the analysis time (given by the duty-cycle) in non-pulsed mode. Furthermore, it was observed that using non-pulsed mode at increasing duty cycles above an optimum value (higher mass load) the ion signals were reduced (see Fig. 2).

Operating conditions retained for the comparison studies are a compromise among the optimum conditions for the different analyte isotopes. In non-pulsed RF mode 500 Pa and 30 W were selected, while in the pulsed RF mode 800 Pa and 100 W were chosen.

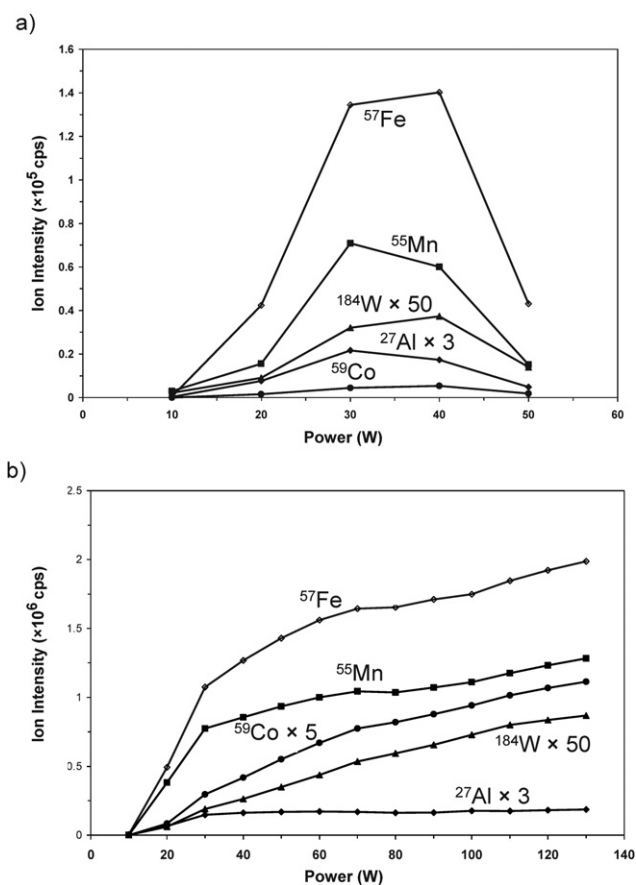


Fig. 4 Ion signal intensities measured for some analytes over the entire afterglow time domain in sample NIST 1262b versus forward power. a) non-pulsed RF mode, pressure: 500 Pa; b) pulsed RF mode, pressure: 700 Pa, pulse width: 2 ms, period: 4 ms.

Spectral interferences and isotopic ratios

Adequate mass resolving power is very important in GD-MS in order to resolve analyte ion signals from isobaric polyatomic species. In our pulsed RF system it is also possible to use the GD source time resolution to further separate analyte ions from polyatomic and discharge gas species because they are formed at different temporal and spatial locations.^{20,21} For instance, Fig. 5a shows the mass spectrum interval between 27.8 and 30.2 Th, measured for the NIST 1262b, using the non-pulsed RFGD-TOFMS at 30 W and 550 Pa. At this mass interval, the ion signals from $^{28}\text{Si}^+$ (Si mass fraction in the NIST 1262b is 0.4%) and from $^{12}\text{C}^{16}\text{O}^+$ are shown. The mass resolving power needed to separate both signals is about 1500 and our non-pulsed RFGD-TOFMS system could partially resolve both peaks; however, a deconvolution procedure would be needed for accurate measurements of the $^{28}\text{Si}^+$ ion signal. Moreover, less abundant Si isotopes at 29 Th and 30 Th have close peaks corresponding to $^{14}\text{N}_2^1\text{H}^+$ and $^{14}\text{N}^{16}\text{O}^+$, respectively. In this latter case, Si analyte ion signals are better resolved from the polyatomic interferences. Therefore, measurement of $^{29}\text{Si}^+$ and $^{30}\text{Si}^+$ ion signals would be recommended to determine Si in the NIST 1262b using the non-pulsed RF-GD-TOFMS, in spite of the much lower abundance of these Si isotopes.

Figs. 5b and 5c show the same region of the mass spectrum measured using the pulsed RFGD-TOFMS system. Fig. 5b shows the mass spectrum collected 30 μs after the end of the GD pulse. In this case, only one peak is observed at 28 Th, which corresponds to $^{28}\text{Si}^+$. Moreover, $^{29}\text{Si}^+$ is not only well resolved from $^{14}\text{N}_2^1\text{H}^+$, but also its $^{29}\text{Si}^+$ is higher than that of $^{14}\text{N}_2^1\text{H}^+$. The ion signals measured at 30 Th are more intense than before (note the difference in the scales) but the relative intensity between $^{29}\text{Si}^+$ and $^{14}\text{N}^{16}\text{O}^+$ is similar to that obtained in non-pulsed RF mode. Furthermore, the isotopic ratios $^{28}\text{Si}^+ / ^{29}\text{Si}^+$ and $^{28}\text{Si}^+ / ^{30}\text{Si}^+$ are 20.80 and 28.27, respectively, which corresponds to a 5% deviation from the natural isotope abundance ratio. On the other hand, Fig. 5c shows the mass spectrum collected 220 μs after the end of the GD pulse. At this later delay time only polyatomic interferences $^{14}\text{N}_2^1\text{H}^+$ and $^{14}\text{N}^{16}\text{O}^+$ are detected at 29 Th and 30 Th, respectively. Probably the presence of these polyatomic signals is due to plasma recombination processes once the plasma temperature in the later afterglow has substantially decreased. This effect has been observed not only for nitrogen containing species but also for other species, such as Ar and C containing species, affecting for instance the Cr ion signals in the afterglow. This example shows how pulsed RF mode requires a careful selection of an appropriate temporal time window for optimised conditions. Under such appropriate time window, ion analyte signals should be more intense and free from spectral interferences, improving the analytical figures of merit that can be achieved using a non-pulsed RFGD-TOFMS system.

The ability to discriminate polyatomic interferences from the analytical ion signals using the temporal resolution offered by the pulsed RF mode is clearly demonstrated when looking at the isotopic ratios. Table 2 collects the theoretical isotopic ratios of the analytes present in the NIST 1262b, as well as the experimental isotopic ratios obtained in pulsed and non-pulsed radiofrequency modes. As can be seen, the isotopic ratios measured using the pulsed mode show higher accuracy than those obtained using the non-pulsed radiofrequency mode and thus indicating lower polyatomic interferences. For example, the isotopic ratio $^{12}\text{C}^+ / ^{13}\text{C}^+$ is deviated 7% from the theoretical value using the pulsed RF mode, while it deviates 87% using the non-pulsed RF mode (due to the presence of $^{12}\text{C}^1\text{H}^+$, *i.e.* the interference not resolved from $^{13}\text{C}^+$). Similarly, $^{40}\text{Ar}^{12}\text{C}^+$ interferes $^{52}\text{Cr}^+$ signal in non-pulsed RF mode. However, in pulsed mode RF this chromium interference can be avoided by selecting an appropriate time window in the afterglow.

Stability, reproducibility and sensitivity

The signal stability was studied over 450 seconds after GD plasma ignition. Fig. 6a and b show the time dependence of the ion signal intensities observed in non-pulsed and pulsed RF modes respectively. A logarithmic scale for the intensity has been used in order to easier visualize in the same graph signals from selected elements (wide range of concentrations) in the sample NIST 1262b. In non-pulsed RF mode (Fig. 6a), a complete mass spectrum is collected every 0.99 s, while in pulsed RF mode it takes about 5.7 s at the selected operating conditions of the TOFMS. The relative standard deviations (RSDs) of the ion signals observed were between 5–20% for all the analyte species.

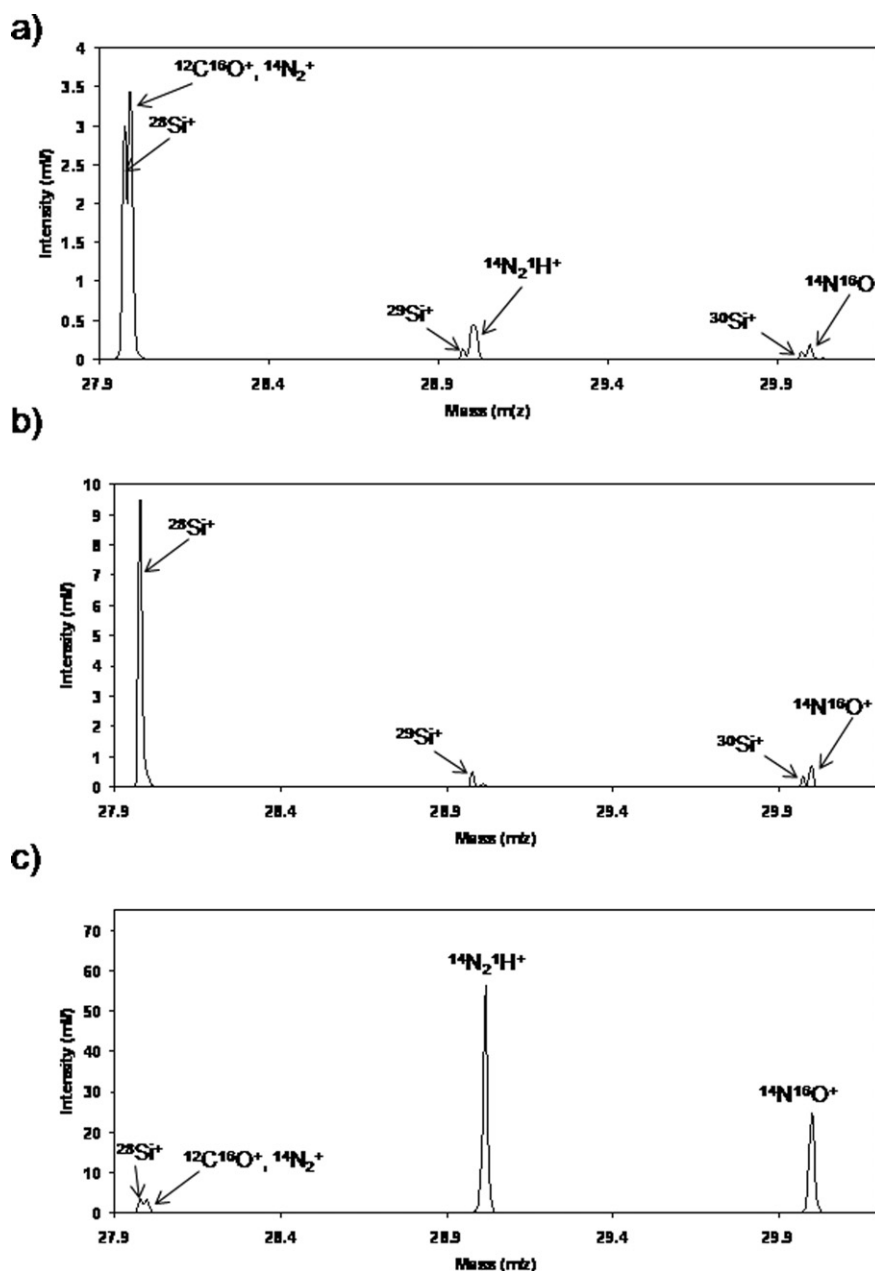


Fig. 5 Mass spectrum between m/z 27.9 and 30.1 of sample NIST 1262b. a) non-pulsed RF mode at 30 W and 550 Pa. b) pulsed RF mode at 100 W, 900 Pa and extracted at 30 μ s after the end of the GD pulse. c) pulsed RF mode at 100 W, 900 Pa extracted at 220 μ s after the end of the GD pulse.

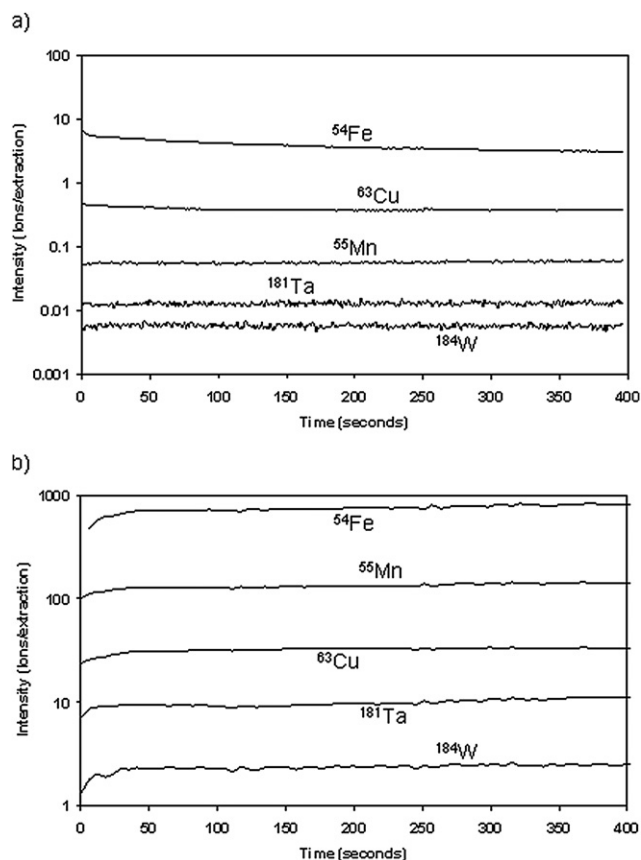
Reproducibility was also estimated for both operating modes. The mean value of the ion signal intensities obtained from 6 different measurements (40 s per measurement) carried out on two different craters (3 measurements/crater), was calculated. Table 3 collects the RSD of the ratio between the analyte ion signals and $^{54}\text{Fe}^+$ (used as internal standard). RSD values are not given for relative ion signals of $^{24}\text{Mg}^+$ and $^{32}\text{S}^+$ in non-pulsed RF mode because these signals are not properly resolved from their interferences ($^{12}\text{C}_2^+$ and $^{16}\text{O}_2^+$, respectively). Also, the high RSD obtained for the ratio $^{12}\text{C}^+ / ^{54}\text{Fe}^+$, in both modes, was proved to be due to the C surface contamination, which results in enhanced C signals on the first measurements carried out on a new crater (non sputtered surface). As can be observed, the calculated RSDs depend on the content of the element in the NIST 1262b and also

on the operating mode (non-pulsed or pulsed RF). For instance, in pulsed RF mode the elements with low content in the sample show higher RSD (see $^{11}\text{B}^+$, $^{24}\text{Mg}^+$ or $^{107}\text{Ag}^+$). In non-pulsed RF mode high RSDs are also obtained for $^{51}\text{V}^+$ or $^{59}\text{Co}^+$, probably due to tailing of $^{40}\text{Ar}^+$ and $^{40}\text{Ar}^1\text{H}^+$ ion signals affecting $^{51}\text{V}^+$ (or the long tail of $^{56}\text{Fe}^+$ ion signal affecting $^{59}\text{Co}^+$).

The sensitivity in $\text{cps}(\mu\text{g g}^{-1})^{-1}$ achieved with the non-pulsed and pulsed RFGD-TOFMS systems was evaluated for the analysis of NIST 1262b. In pulsed RF mode two ways of data treatment have been considered: (i) the ion signal of each isotope is its area under the afterglow and (ii) the ion signal of each isotope corresponds to its maximum value in the afterglow. Fig. 7 shows the sensitivity obtained using the non-pulsed and the pulsed RFGD-TOFMS systems for a wide selection of

Table 2 Isotopic ratios calculated in non-pulsed RF and pulsed RF modes

Isotopic Ratios	Theoretical ratio	Experimental ratio Pulsed RF mode	Experimental ratio Non-pulsed RF mode
$^{11}\text{B}^+ / ^{10}\text{B}^+$	4.03	4.3	6.1
$^{12}\text{C}^+ / ^{13}\text{C}^+$	89.09	82.5	11.2
$^{24}\text{Mg}^+ / ^{25}\text{Mg}^+$	7.90	8.0	—
$^{28}\text{Si}^+ / ^{29}\text{Si}^+$	19.75	20.8	—
$^{28}\text{Si}^+ / ^{30}\text{Si}^+$	29.75	28.3	—
$^{32}\text{S}^+ / ^{33}\text{S}^+$	126.69	142.7	58.7
$^{32}\text{S}^+ / ^{34}\text{S}^+$	22.57	23.5	29.9
$^{46}\text{Ti}^+ / ^{47}\text{Ti}^+$	1.09	1.3	0.9
$^{48}\text{Ti}^+ / ^{46}\text{Ti}^+$	9.26	9.3	1.5
$^{48}\text{Ti}^+ / ^{47}\text{Ti}^+$	10.10	12.3	1.3
$^{90}\text{Zr}^+ / ^{91}\text{Zr}^+$	4.59	4.6	2.3
$^{120}\text{Sn}^+ / ^{118}\text{Sn}^+$	1.35	1.4	1.4
$^{118}\text{Sn}^+ / ^{119}\text{Sn}^+$	2.82	3.0	1.9
$^{120}\text{Sn}^+ / ^{119}\text{Sn}^+$	3.80	4.5	2.7
$^{121}\text{Sb}^+ / ^{123}\text{Sb}^+$	1.34	1.3	1.4
$^{184}\text{W}^+ / ^{182}\text{W}^+$	1.17	1.2	1.2
$^{186}\text{W}^+ / ^{182}\text{W}^+$	1.09	1.1	1.1

**Fig. 6** Intensity *versus* time measured for some isotopes of sample NIST 1262b. a) non-pulsed RF mode 30 W, 500 Pa. b) pulsed RF mode 100 W, 800 Pa (the intensities correspond to the average of the intensities measured over the entire afterglow time domain).

analytes present in the reference sample NIST 1262b. A significant sensitivity improvement is clearly achieved in pulsed RF mode for most elements. In general terms, the sensitivity

obtained for the different analytes of NIST 1262b using the non-pulsed RF mode lied in the range $0.20\text{--}40\text{ cps}(\mu\text{g g}^{-1})^{-1}$ while in pulsed RF mode the sensitivity for the different elements was enhanced to values from 6 to $165\text{ cps}(\mu\text{g g}^{-1})^{-1}$, measuring the average ion signal or to values $23\text{--}415\text{ cps}(\mu\text{g g}^{-1})^{-1}$ if maximum ion signal in the afterglow is measured.

Interestingly, the most substantial enhancement was observed for low “mass/charge” ratios ($<75\text{ Th}$) ion signals, probably due to mass dependence of the ion transport efficiency into the TOFMS. On the other hand, the low absolute sensitivities observed for $^{48}\text{Ti}^+$ and $^{51}\text{V}^+$ might be attributed to the long tail produced by the very high intensity $^{40}\text{Ar}^+$ signal. Fortunately, the sensitivity obtained for the two isotopes in pulsed RF mode is greatly improved (due to temporal separation of the analyte ions from the discharge interfering gas ion species).

In order to investigate further possible reasons for the observed sensitivity enhancement when using the pulsed RF mode, the sputtering rates were evaluated. The averaged applied power in pulsed RF mode ($50\text{ W} = 100\text{ W} \times 50\%$ duty cycle) is about 1.6 times higher than the applied power in non-pulsed RF mode (30 W). Similarly, the sputtering rate calculated for each operating mode was $5.5 \pm 0.3\ \mu\text{g s}^{-1}$ and $6.8 \pm 0.9\ \mu\text{g s}^{-1}$ in non-pulsed and pulsed mode respectively, indicating a ratio, $q_{\text{pulsed}}/q_{\text{non-pulsed}}$ of only about 1.2 ± 0.2 . Therefore, higher sputtering rate in pulsed RF mode does not fully explain sensitivity enhancement (while the pulsed/non-pulsed signal ratio is usually greater than 4). Higher ionization efficiency in the afterglow of the pulsed RFGD and/or higher ion transport efficiency into the TOFMS also contribute to the observed enhanced sensitivity in the pulsed RF mode.

The limits of detection (LODs) calculated for both operating modes, as three times the standard deviation of the background divided by the slope of the calibration curve, are given in Table 4. The calibration curve was obtained using four reference materials with similar iron matrices (see Table 1). The background was measured in the baseline at the left of the corresponding ion signal peak. Table 4 lists the LODs, calculated for the analytes of the reference sample NIST 1262b, in non-pulsed and the pulsed RF modes and demonstrates that the LODs in non-pulsed RF mode vary from 0.5 up to $46\ \mu\text{g g}^{-1}$ depending on the element. However, using pulsed RF mode the LODs were better, varying from 0.2 up to $12\ \mu\text{g g}^{-1}$.

Qualitative in-depth profile analysis capabilities

To evaluate depth profile analysis capabilities of non-pulsed and pulsed RFGD-TOFMS systems a coated sample, consisting of a Zn/Ni coating of about $2\ \mu\text{m}$ on steel was analyzed. The experiments were carried out at optimum conditions to obtain adequate crater shapes for depth profiling (craters with flat bottoms and vertical walls). Optimum conditions were achieved at 500 Pa and 25 W in non-pulsed RF mode, and at 800 Pa and 100 W in pulsed RF mode. Fig. 8a and b illustrate the qualitative depth profiles of the Zn/Ni coating on steel obtained using both non-pulsed (8a) and pulsed RF (8b) modes, respectively. In non-pulsed RF mode we observed some surface contamination that contribute to the ion signals of $^{27}\text{Al}^+$ and $^{52}\text{Cr}^+$ due to spectral interference from $^1\text{H}^{12}\text{C}^{14}\text{N}^+$ and $^{40}\text{Ar}^{12}\text{C}^+$, respectively. On the other hand, these spectral interferences are better resolved using

Table 3 Relative standard deviation (RSD) of the relative ion signal intensities ($^{54}\text{Fe}^+$ as internal standard). Sample NIST 1262b. $N = 6$ measurements

Element	Isotope	RSD (%) Non-pulsed RF mode	RSD (%) Pulsed RF mode
B	11	9	12
Mg	24	—	28
Al	27	6	2
Si	28	—	6
P	31	7	5
S	32	—	6
Ti	48	8	6
V	51	22	5
Cr	52	12	15
Mn	55	5	2
Co	59	18	3
Ni	60	16	4
Cu	63	6	14
As	75	11	7
Zr	90	10	11
Nb	93	7	10
Mo	98	3	7
Ag	107	9	15
Sn	120	12	9
Sb	121	9	2
Ta	181	13	4
W	184	14	3
Pb	208	7	9

the pulsed-RF mode (evaluating the data from the afterglow time domain as previously described in Fig. 5b and c), and do not contribute to the analyte ion signals. Ion signals from the pre-peak and plateau do not allow this temporal discrimination of

the analyte ion signals from the spectral interferences and in addition lower sensitivity is achieved.

As can be seen in the qualitative depth profiles, comparative sputtering times (Fig. 8) were needed to reach the coating interface (slightly higher in pulsed RF mode) and similar depth resolution was achieved. However, the ion signal intensities were

Table 4 LODs calculated in $\mu\text{g g}^{-1}$ for non-pulsed RF (operating conditions: 500 Pa, 30 W) and for pulsed RF mode (operating conditions: 800 Pa, 100 W, 2 ms pulse width and 50% duty cycle)

Isotope	Non-pulsed RF mode	Pulsed RF mode
^{11}B	0.8	0.3
^{24}Mg	0.5	0.2
^{27}Al	2.1	0.3
^{28}Si	6.4	1.9
^{31}P	2.4	1.6
^{32}S	1.6	1.0
^{48}Ti	46	2.3
^{51}V	25	1.1
^{52}Cr	8.9	1.0
^{55}Mn	7.8	5.5
^{59}Co	46	8.3
^{60}Ni	19	12
^{63}Cu	8.2	1.2
^{75}As	2.5	0.8
^{90}Zr	55	2.2
^{93}Nb	42	1.6
^{95}Mo	6.8	0.2
^{107}Ag	0.6	0.5
^{118}Sn	1.9	0.6
^{121}Sb	1.1	0.8
^{181}Ta	15	0.5
^{184}W	5.9	0.9
^{208}Pb	0.8	0.4

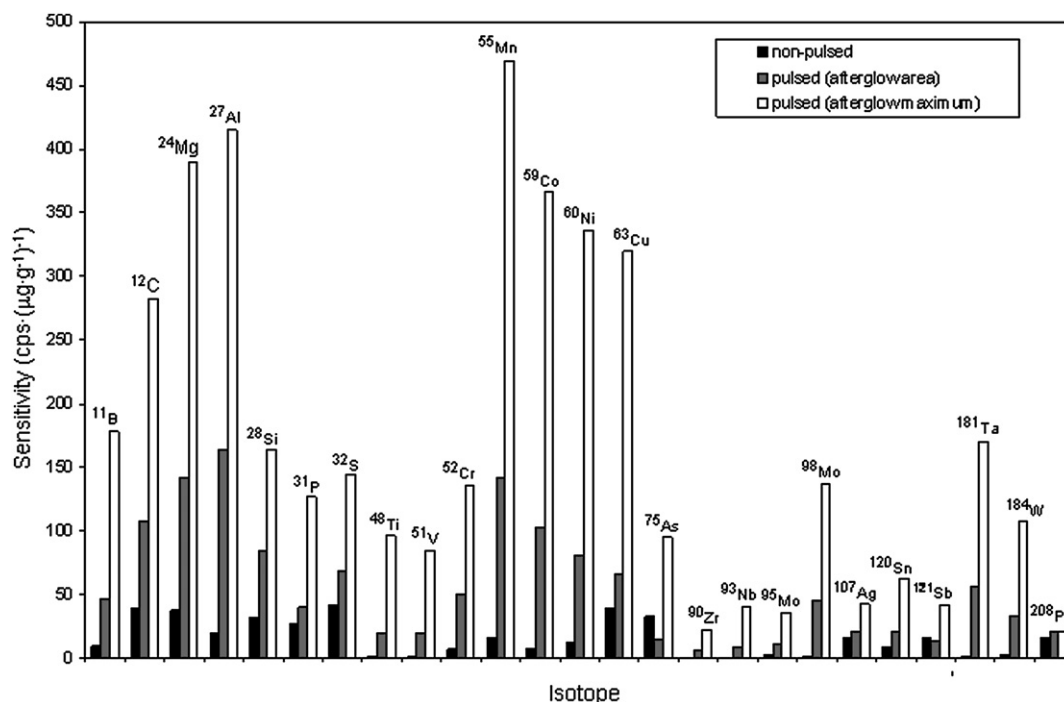


Fig. 7 Sensitivities obtained for the major isotopes present in the sample NIST 1262b in non-pulsed RF mode, in pulsed RF mode considering the intensity as the average of the intensities extracted over the afterglow, and in pulsed RF mode using the intensity extracted at the maximum of the afterglow.

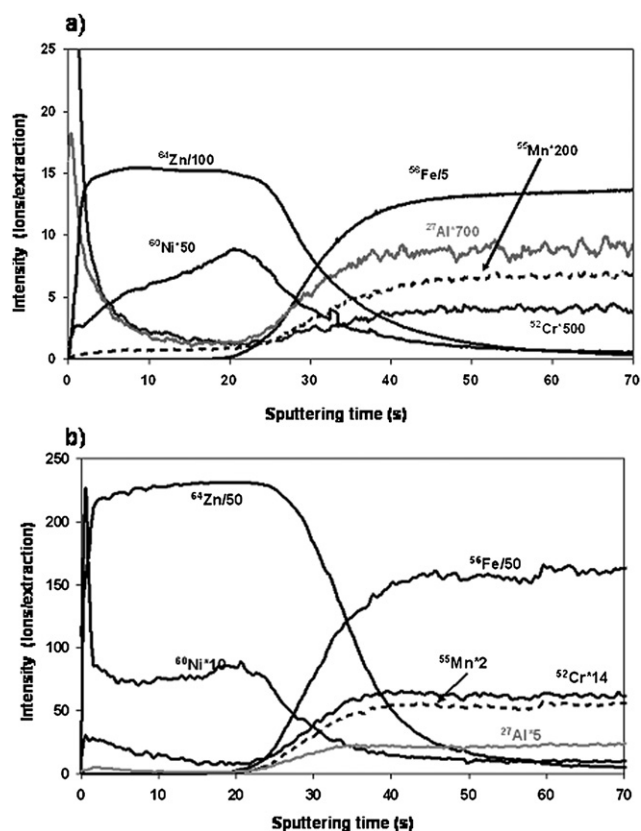


Fig. 8 Qualitative in-depth profile of a Zn/Ni coating on steel. (a) non-pulsed RF mode at 500 Pa, 25 W. (b) pulsed RF mode at 800 Pa, 100 W (pulse width: 2 ms, period: 4 ms). The different delay times chosen for the analytes after the end of the GD pulse were 132 μs for $^{64}\text{Zn}^+$, 264 μs for $^{27}\text{Al}^+$, $^{55}\text{Mn}^+$, $^{56}\text{Fe}^+$, $^{52}\text{Cr}^+$ and $^{60}\text{Ni}^+$. The integration time was 33 μs for all the isotopes except for $^{52}\text{Cr}^+$ and $^{60}\text{Ni}^+$ where 66 μs was chosen.

much higher in the pulsed RF mode. As can be observed, both operating modes were adequate for the depth profiling of the analysed relatively thick coating. However, the higher sensitivity, needed for the analysis of trace elements will require the use of the pulsed RFGD-TOFMS system.

Conclusions

Non-pulsed and pulsed-radiofrequency glow discharges have been investigated and compared as ion sources for an orthogonal time-of-flight mass spectrometer. The operating conditions were optimised for the analysis of a certified reference steel sample, using both non-pulsed and the pulsed RF modes. The highest analyte ion signals in the pulsed RF mode were found in the afterglow; therefore, ion signals for data treatment were collected from this time window.

The study of applied power dependence has shown a different behaviour for both operation modes, which could be attributed to enhanced ion transmission to the TOFMS in the case of the pulsed RF operation mode. Further studies are needed to investigate the difference in the ion transport efficiency from the GD plasma into the mass spectrometer. In this context, optical

emission measurements with spatial and temporal resolution will be carried out to investigate the distribution of the Ar^m and analyte species in the plasma plume.

Results also showed that in pulsed RF mode certain isobaric molecular interferences can be avoided by choosing a proper time window within the afterglow. Long term stability and reproducibility were similar for both operating modes. Importantly for analytical purposes, the LODs were significantly improved using the pulsed RF mode, probably due to higher ionization efficiency in the afterglow domain and better ion transport into the TOFMS.

Acknowledgements

This work was supported by FP6 Contract STREP-NMP, N^o 032202. J. Pisonero acknowledges financial support from "Ramon y Cajal" Research Program of the Ministry of Science and Innovation of Spain.

References

- 1 R. K. Marcus and J. A. C. Broekaert, *Glow Discharge Plasmas in Analytical Spectroscopy*, John Wiley & Sons Ltd., England, 2003.
- 2 F. Chartier and M. Tabarant, *Spectra Analyse*, 2008, **37**, 34–41.
- 3 M. R. Winchester and R. Payling, *Spectrochim. Acta, Part B*, 2004, **59**, 607–666.
- 4 J. Pisonero, J. M. Costa, R. Pereiro, N. Bordel and A. Sanz-Medel, *Anal. Bioanal. Chem.*, 2004, **379**, 17–29.
- 5 R. Jäger, J. S. Becker, H.-J. Dietze and J. A. C. Broekaert, *Fresenius J. Anal. Chem.*, 1997, **358**, 214–217.
- 6 J. Pisonero, J. M. Costa, R. Pereiro, N. Bordel and A. Sanz-Medel, *Anal. Bioanal. Chem.*, 2004, **379**, 658–667.
- 7 A. Bogaerts and R. Gijbels, *Spectrochim. Acta, Part B*, 1998, **53**, 1–42.
- 8 A. Bogaerts and R. Gijbels, *Spectrochim. Acta, Part B*, 2000, **55**, 263–278.
- 9 A. C. Muñiz, J. Pisonero, L. Lobo, C. Gonzalez, N. Bordel, R. Pereiro, A. Tempez, P. Chapon, N. Tuccitto, A. Licciardello and A. Sanz-Medel, *J. Anal. At. Spectrom.*, 2008, **23**, 1239–1246.
- 10 M. Hohl, A. Kanzari, J. Michler, T. Nelis, K. Fuhrer and M. Gonin, *Surf. Interface Anal.*, 2006, **38**, 292–295.
- 11 W. W. Harrison, C. Yang and E. Oxley, *Anal. Chem.*, 2001, **73**, 480A–487A.
- 12 D. Fliegel, K. Fuhrer, M. Gonin and D. Günther, *Anal. Bioanal. Chem.*, 2006, **386**, 169–179.
- 13 A. Solà-Vázquez, A. Martín, J. M. Costa-Fernández, R. Pereiro and A. Sanz-Medel, *Anal. Chem.*, 2009, **81**, 2591–2599.
- 14 N. Tuccitto, L. Lobo, A. Tempez, I. Delfanti, P. Chapon, S. Canulescu, N. Bordel, J. Michler and A. Licciardello, *Rapid Commun. Mass Spectrom.*, 2009, **23**, 549–556.
- 15 A. Tempez, N. Bordel, M. Hohl, L. Lobo, J. Orphal, C. Diplasu, A. Surmeian, M. Ganciu and T. Nakamura, *Proceedings of the 18th International Symposium on Plasma Chemistry*, K. Tachibana, Kyoto, Japan, ISBN 978-4-9903773-1-1, 267–271, 2007.
- 16 E. Oxley, C. Yang, J. Liu and W. W. Harrison, *Anal. Chem.*, 2003, **75**, 6478–6484.
- 17 M. Hohl *et al.* "Internal report of EMDPA project" 2008. European Project (STREP 032202 EMDPA).
- 18 A. Martín, A. Martínez, R. Pereiro, N. Bordel and A. Sanz-Medel, *Spectrochim. Acta Part B*, 2007, **62**, 1263–1268.
- 19 K. Wagatsuma, T. Saka, M. Yamaguchi and K. Ito, *J. Anal. At. Spectrom.*, 2002, **17**, 1359–1362.
- 20 R. E. Steiner, C. L. Lewis and V. Majidi, *J. Anal. At. Spectrom.*, 1999, **14**, 1537–1541.
- 21 J. A. Klinger, C. M. Barshick and W. W. Harrison, *Anal. Chem.*, 1991, **63**, 2571–2576.